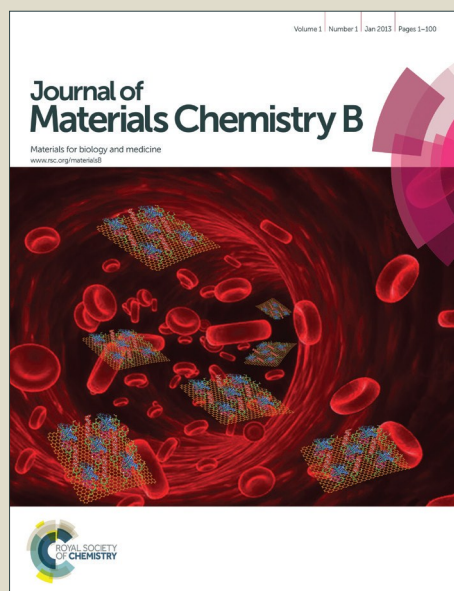


Journal of Materials Chemistry B

Accepted Manuscript



This is an *Accepted Manuscript*, which has been through the Royal Society of Chemistry peer review process and has been accepted for publication.

Accepted Manuscripts are published online shortly after acceptance, before technical editing, formatting and proof reading. Using this free service, authors can make their results available to the community, in citable form, before we publish the edited article. We will replace this *Accepted Manuscript* with the edited and formatted *Advance Article* as soon as it is available.

You can find more information about *Accepted Manuscripts* in the [Information for Authors](#).

Please note that technical editing may introduce minor changes to the text and/or graphics, which may alter content. The journal's standard [Terms & Conditions](#) and the [Ethical guidelines](#) still apply. In no event shall the Royal Society of Chemistry be held responsible for any errors or omissions in this *Accepted Manuscript* or any consequences arising from the use of any information it contains.



Journal Name

ARTICLE

Microgels with tunable affinity-controlled protein release via desolvation of self-assembled peptide nanofibers

Margaret M. Fettis^{a,*}, Yaohua Wei^{a,*}, Antonietta Restuccia^a, Justin Kurian^c, Shannon M. Wallet^b, and Gregory A. Hudalla^{a,†}

Received 00th January 20xx,
Accepted 00th January 20xx

DOI: 10.1039/x0xx00000x

www.rsc.org/

With a growing number of bioactive protein drugs approved for clinical use each year, there is increasing need for vehicles for localized protein delivery to reduce administered doses, prevent off-target activity, and maintain protein bioactivity. Ideal protein delivery vehicles provide high encapsulation efficiency of bioactive drug, enable fine-tuning of protein release profiles, are biocompatible, and can be administered via minimally-invasive routes. Here we developed an approach to create micron-sized hydrated gels (i.e. "microgels") for protein delivery that fulfill these requirements via desolvation of self-assembled β -sheet peptide nanofibers. Specifically, aqueous solutions of peptide nanofibers were diluted under stirring conditions in a "desolvating agent", such as ethanol, which is miscible with water but poorly solvates peptides. The desolvating agent induced nanofiber physical crosslinking into microgels that retained β -sheet secondary structure and were stable in aqueous solutions. Microgels did not activate dendritic cells *in vitro*, suggesting they are biocompatible. Peptide nanofibers and proteins having similar non-solvent immiscibility properties were co-desolvated to produce protein-loaded microgels with loading efficiencies of ~85%. Encapsulated bioactive proteins rapidly diffused into bulk aqueous media, as expected for hydrated gels. Modifying peptide nanofibers with a protein-binding ligand provided tunable affinity-controlled protein release. Biocompatible microgels formed via desolvation of self-assembled peptide nanofibers are therefore likely to be broadly useful for as vehicles for localized delivery of bioactive proteins, as well as other therapeutic molecules.

1. Introduction

The advent of recombinant protein production with human insulin in the late 1970s and protein engineering in the early 1980s has led to increasing interest in proteins as therapeutics and diagnostic agents, with more than 125 FDA-approved protein drugs in current clinical use and many more in development.¹ In part, this is because protein drugs can perform complex functions that cannot be achieved by small molecules, their mode of action is highly specific and therefore reduces potential for deleterious side effects, and their amino acid components are natural molecules that are well-tolerated and can be readily metabolized. In addition, progress in gene synthesis and DNA recombination, as well as protein expression and purification, have led to significant improvements in large-scale protein production. Despite these advantages, however, the number of failed protein therapeutics and diagnostics greatly exceeds current successes,² in part because of key challenges related to unwanted activity at secondary 'non-target' sites, immunogenicity arising from repetitive high dose

administration, and limited serum stability. To address these challenges, there is growing interest in vehicles that can be administered via minimally-invasive routes to create localized depots of protein drugs that are released at tightly controlled doses.

Hydrogels, which are highly hydrated networks of crosslinked natural or synthetic polymers, are receiving increasing attention as vehicles for protein drug delivery because they are biocompatible, their highly hydrated nature and mild fabrication conditions are favorable for maintaining protein bioactivity, and their chemical composition can be tailored to modulate protein drug release profiles.³ Hydrogels based on peptides and peptide analogs that self-assemble into nanofibers are widely used as vehicles for delivery of proteins, cells, and other therapeutic molecules, because they can fulfill these requirements.⁴⁻⁷ In particular, nanofibers based on synthetic peptides that self-assemble into β -sheets can be fabricated into hydrogels under mild aqueous conditions that are favorable for maintaining protein bioactivity, and are often biocompatible with various cells and tissues.^{7, 8} In addition, self-assembled β -sheet peptide nanofibers often induce minimal inflammation, and elicit weak or no adaptive immunity directed against the peptide itself, despite being foreign to the host.⁹⁻¹⁴ The chemical composition and physical features of biomaterials based on self-assembled peptide nanofibers can also be precisely modified during peptide synthesis or hydrogel fabrication to tune protein release profiles. For example, hydrogel pore size influences rate of protein release.^{15, 16} Varying self-assembling peptide charge provides electrostatic control of protein release.^{17, 18} Modifying self-assembling peptides with ligands that bind to proteins directly or

^a J. Crayton Pruitt Family Department of Biomedical Engineering, 1275 Center Drive, University of Florida, Gainesville, FL, 32611

^b Department of Oral Biology, 1395 Center Drive, University of Florida, Gainesville, FL, 32610

^c Department of Biochemistry and Molecular Biology, 1200 Newell Drive, University of Florida, Gainesville, FL, 32610

† Corresponding author - ghudalla@bme.ufl.edu

* Authors contributed equally

Electronic Supplementary Information (ESI) available: [Supplementary Figures 1-7]. See DOI: 10.1039/x0xx00000x

indirectly (e.g. via heparin or biotin) can provide affinity-dependent modulation of protein release.¹⁹⁻²³

One practical challenge of using macroscopic hydrogels for protein delivery is that they often need to be administered via invasive means, such as surgical implantation, which greatly increases patient susceptibility to infection and other associated complications. Notably, self-assembled peptide nanofibers can often be engineered to gel *in situ* or undergo shear-thinning and recovery, which allows for minimally-invasive administration via syringe injection.^{13, 24-27} However, the fluidity of shear-thinning and *in situ* gelling biomaterials is also likely to render them susceptible to dissolution or fracture in biological fluids, as well as lead to gelation into non-uniform shapes with ill-defined release profiles *in vivo*. Alternatively, micron-sized polymeric vehicles that can be fabricated *in vitro* and directly administered *in vivo* without the need for *in situ* gelation or shear-thinning are advantageous for protein delivery because they are more robust under biological conditions, and can therefore provide more reproducible and well-defined protein release profiles.²⁸ Various emulsion and microfluidic methods are amenable to fabricating micron-sized hydrogels (i.e. "microgels") from self-assembled peptide or protein nanofibers,²⁹⁻³³ with the former providing potential for scalability and the latter providing exceptional control of microgel size, and in turn drug release profiles. However, microgels fabricated from self-assembled peptide or protein nanofibers have primarily been investigated as vehicles for cell or small molecule drug delivery, with much less attention to protein drug delivery to date.

Here, we demonstrate a method to fabricate microgels for protein drug delivery via desolvation of self-assembled β -sheet peptide nanofibers. Since the late 1970s, desolvation has been used to fabricate nanoparticles for drug delivery from proteins, such as albumin and gelatin.^{34, 35} The process utilizes a "desolvating agent" or "non-solvent", such as salts, ethanol, or acetone, which alters the osmotic action of water on macromolecules, leading to their precipitation, aggregation, and coacervation.³⁶ We proposed that diluting an aqueous solution of β -sheet peptide nanofibers in a non-solvent under stirring conditions would induce nanofiber entanglement into physically-crosslinked microgels. In particular, micron-sized particles would result due to the larger size and high aspect ratio of nanofibers (nm in one dimension, 100s of nm to μ m in the other) when compared to proteins, which typically yield nanoparticles. In addition, peptide nanofibers would yield stable, physically-crosslinked microgels driven by their propensity for non-covalent inter-fiber interactions, thereby eliminating the need for glutaraldehyde or heat-denaturation crosslinking that is often necessary to stabilize protein nanoparticles fabricated via desolvation.³⁷ Toward this end, we report on the desolvation of β -sheet nanofibers of the synthetic peptide, Ac-QQKFQFQQ-Am ("Q11"), which self-assembles under mild aqueous buffered conditions at μ M concentrations, and can form self-supporting hydrogels above a critical concentration (\sim 5-10 mM).³⁸ Q11 nanofibers are particularly useful as materials for biomedical applications because they are biocompatible, induce minimal inflammation, and are non-immunogenic.^{9, 10} Specifically, we characterized the influence of non-solvent type and Q11 concentration on desolvation. In addition, we compared desolvation of Q11 β -sheet nanofibers to that of other zwitterionic synthetic β -sheet fibrillizing peptides that form self-supporting hydrogels under mild aqueous conditions, Ac-RADARADARADA-Am (RADA16, *PuraMatrix*TM)³⁹ and Ac-FKFEFKFE-Am (KFE8).⁴⁰ Finally, we assessed co-desolvation of peptide nanofibers and proteins having similar molecular

composition, and thus similar non-solvent immiscibility properties, as a means to create micro-scale protein drug delivery vehicles with high encapsulation efficiency and tunable release of bioactive cargoes.

2. Results and discussion

2.1 Microgel fabrication via desolvation of self-assembled peptide nanofibers

Q11 nanofibers were fabricated into microgels via desolvation (Figure 1), a 3-step batch process involving Q11 self-assembly into nanofibers under aqueous buffered conditions (Figure 1a, top), dilution of Q11 nanofibers in excess non-solvent (e.g. ethanol, "EtOH") (Figure 1a, center), and recovery of microgels from non-solvent via centrifugation followed by resuspension in aqueous buffer (Figure 1a, bottom). Q11 in PBS self-assembled into nanofibers (Figure 1b, left) as visualized with TEM, consistent with previous reports.³⁸ Under a fluorescent microscope, Q11 nanofibers stained with Thioflavin T (ThT), a β -sheet fibril binding dye,⁴⁵ appeared as amorphous fluorescent flocculates (Figure 1b, right), suggesting the presence of soluble and loosely associated nanofibers at the micro-scale prior to desolvation.

Following dilution of aqueous Q11 nanofibers in excess EtOH under stirring conditions, spherical particles \sim 10 μ m in diameter were observed with SEM (Figure 1c, left). The surface of these particles appeared relatively smooth when visualized via SEM, similar to microgels fabricated from lysozyme fibers.³⁰ Particles resulting from diluting aqueous Q11 nanofibers in excess EtOH under stirring conditions were fluorescent in the presence of ThT (Figure 1c, right), suggesting that the β -sheet secondary structure of Q11 was maintained during step 2 of the desolvation process.

Particle size, morphology, and ThT fluorescence were maintained following centrifugation, removal of non-solvent supernatant, and resuspension in PBS (Figure 1d, left), suggesting that the desolvation process induced physical crosslinking of Q11 β -sheet nanofibers into microgels that are stable under aqueous conditions. Q11 was recovered from the desolvation process in high yield, given that ThT fluorescence correlated with Q11 concentration in solution (Supplemental Figure 2) and the intensity of Q11 microgels recovered following desolvation was similar to that of Q11 nanofibers prior to desolvation (Figure 1d, right).

We further characterized the physicochemical properties of the recovered microgels using TEM, CD, and zeta potential analysis. Transmission electron micrographs collected after the desolvation process demonstrated that the recovered microgels had a nanofibrillar architecture (Figure 1e and f), confirming observations made via staining with ThT (Figure 1d, left). In addition, circular dichroism spectra collected before and after desolvation demonstrated that the recovered microgels had a β -sheet secondary structure, indicated by a minimum at 222 nm, which was similar to that of Q11 nanofibers that had not been subjected to desolvation (Figure 1g). It should be noted that observed differences in the CD spectra of Q11 microgels and nanofibers may be due to subtle changes in nanofiber secondary structure induced via desolvation, or due to differences in refraction of light by samples containing micron-sized, heterogeneous particles versus diffuse nanofibers. Finally, the zeta potential of Q11 before and after desolvation was comparable, having values of 14.36 +/- 0.89 mV and 13.60 +/- 1.03 mV, respectively.

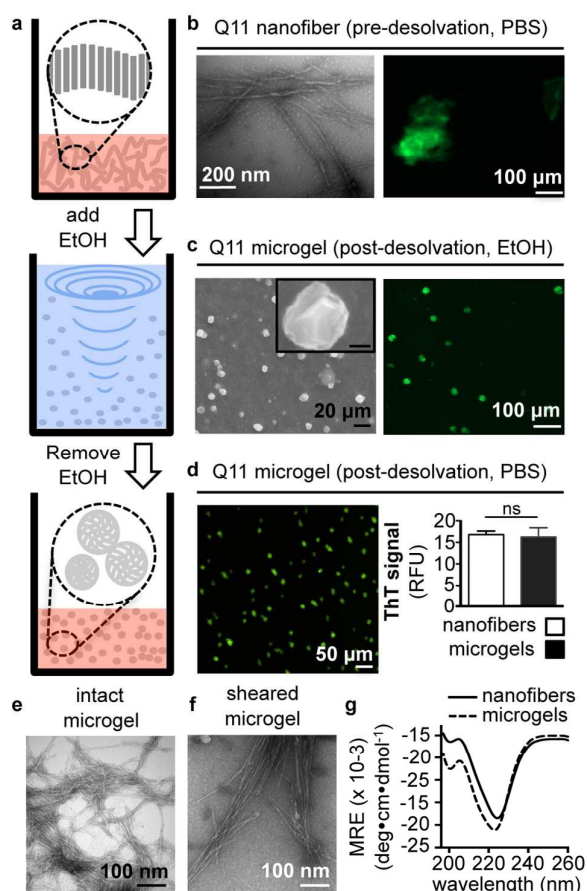


Figure 1. Microgel fabrication via desolvation of Q11 nanofibers. a) Schematic representation of the 3-step desolvation process for fabricating microgels from peptide nanofibers. First, peptides dissolved in aqueous buffer self-assemble into nanofibers (top). Then, dilution of peptide nanofibers in ethanol (EtOH) “non-solvent” under stirring conditions produces microgels (middle). Finally, microgels are recovered via centrifugation and resuspended in aqueous buffer for subsequent use (bottom). b) Transmission electron micrograph of Q11 nanofibers (left) and fluorescent photomicrograph of ThT-stained Q11 nanofibers (right). c) Scanning electron micrograph of Q11 microgels (left) and fluorescent photomicrograph of ThT-stained Q11 microgels (right) in ethanol prior to centrifugation and resuspension in aqueous buffer. d) Fluorescent photomicrograph of ThT-stained Q11 microgels (left) and ThT fluorescence intensity (right) after centrifugation and resuspension of microgels in PBS. “ns” denotes $p > 0.05$ between indicated groups. e-f) Transmission electron micrographs of (e) intact Q11 microgels, and (f) sheared Q11 microgels. g) Circular dichroism of Q11 nanofibers (solid line) and microgels fabricated via desolvation of Q11 (dashed line).

Taken together, these data demonstrated that the 3-step desolvation method outlined in Figure 1a can be used to fabricate microgels from Q11 nanofibers, and that these microgels are stable under aqueous conditions. Fibrillar morphology and surface potential of Q11 nanofibers were retained following desolvation, with the latter suggesting that the microgels may have some propensity for aggregation under aqueous conditions. Although not

investigated here, microgel aggregation could likely be minimized in future efforts by modifying the primary sequence of Q11 to include additional cationic or anionic residues that increase the zeta potential magnitude. Additionally, any residual non-solvent, which may negatively impact microgel biocompatibility or drug release properties, could likely be reduced by introducing evaporation or freeze-drying processes into the existing method. The observation that Q11 nanofiber desolvation provides high-yield recovery of peptide feedstocks used for the production of stable microgels at the bench-scale is noteworthy, given the high cost associated with peptide synthesis and purification. Thus, the batch desolvation method outlined in Figure 1a may provide a scalable and cost effective method for fabricating microgels for use in various applications.

2.2 Influence of peptide concentration, non-solvent properties, and peptide sequence on microgel fabrication via desolvation

Microgel size was dependent on Q11 concentration (Figure 2). In particular, at concentrations below 0.1 mM, which is likely at or near the minimum fibrillization concentration for Q11 as determined by ThT fluorescence (Supplemental Figure 2), no microgels were observed (data not shown). Over the concentration range of 0.1–0.5 mM, microgel size increased with Q11 concentration, such that 0.1 mM, 0.25 mM, and 0.5 mM aqueous buffered solutions of Q11 yielded microgels having diameters of $5 \pm 2 \mu\text{m}$, $7.5 \pm 2 \mu\text{m}$, and $10 \pm 2.5 \mu\text{m}$, respectively (Figure 2a–c). At concentrations above 0.5 mM, however, microgel size was less dependent on Q11 concentration, leading to a maximum microgel diameter range of $12.5 \pm 3 \mu\text{m}$ at a concentration of 1 mM Q11 (Figure 2a–c). One possible explanation for the leveling off of microparticle size with increasing Q11 concentration may be the existence of a concentration threshold at given processing conditions (e.g. non-solvent type, PBS:non-solvent ratio, stir speed) above which there is an increase in total number of microgels formed, rather than a resultant increase in microgel diameter. Such correlations between processing conditions, microgel number, and microgel size may be worthy of future investigation, but are beyond the scope of this report. Nonetheless, when compared to fabrication of Q11 microgels via oil-in-water emulsion, which required Q11 concentrations $\geq 10 \text{ mM}$,²⁹ the desolvation process presented here required Q11 concentrations of 0.1–1 mM. Thus, desolvation not only maximizes peptide feedstock use via high yield recovery (Figure 1d), but also reduces the quantity of synthetic peptide needed by orders of magnitude, which is ideal for scalable microgel production. One potential limitation, however, is that the polydispersity of microgels formed via desolvation is greater than that afforded by microfluidic approaches,^{30,31} instead providing diameter variability that is similar to established oil-in-water emulsion methods.²⁹ In addition, the range of microgel sizes that can be produced via desolvation is much smaller than what can be achieved with oil-in-water emulsion or microfluidic methods,^{29–31} likely because Q11 concentrations must be maintained below the nanofiber sol-gel transition concentration in aqueous buffer ($\sim 3\text{--}5 \text{ mM}$ for Q11) during the desolvation process. This aspect may be improved in the future by modifying the desolvation process to leverage Q11 concentrations spanning the soluble nanofiber and gel range. Nonetheless, this batch process can be used to fabricate microgels with tailored diameters that can be tuned by simply varying peptide

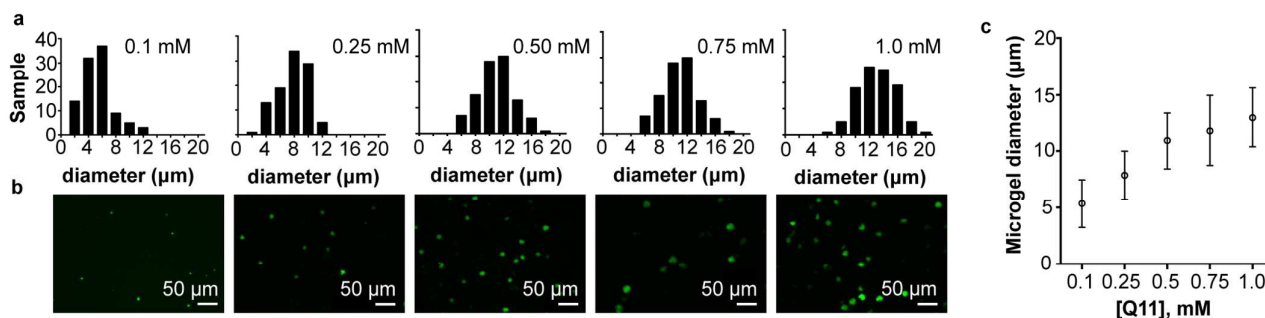


Figure 2. Influence of Q11 concentration on microgel size. a) Histograms of microgel diameter at different Q11 concentrations, (b) fluorescent photomicrographs of ThT-stained microgels at each Q11 concentration, and (c) average and standard deviation of Q11 microgel diameter as a function of Q11 concentration.

concentration, and therefore may provide large-scale production capabilities that are difficult to achieve with flow-based methods for monodisperse microgel production.⁴⁶

Next, we characterized fabrication of microgels from self-assembled peptide nanofibers using various non-solvents (Figure 3). In particular, acetone as non-solvent (Figure 3a) yielded microgels having sizes and spherical morphologies similar to those fabricated using ethanol as non-solvent (Figure 2b). In contrast, methanol and isopropanol desolvated Q11 nanofibers into micron-sized particulates with more irregular morphologies (Figure 3b-c) than those produced by ethanol or acetone (Figure 2b and 3a), and the particulates formed with methanol were typically larger than those formed with any other solvent (Figure 3b). Taken together, data in figure 3 demonstrated that various common non-solvents induced a significant change in micro-scale Q11 nanofiber morphology when compared to that of Q11 nanofibers in aqueous buffer prior to desolvation (Figure 1b, right), however only ethanol and acetone were amenable to microgel fabrication with the particular desolvation conditions employed here (i.e. non-solvent:PBS ratio, mixing speed). From a mechanistic perspective, these observed differences may in part be related to the properties of each non-solvent. For instance, as the dielectric constant of a solution decreases it becomes a poorer solvent for proteins.⁴⁷ Thus, the larger size of microgels fabricated with methanol may be due to it having the highest dielectric constant, and therefore lowest desolvation efficiency, of the non-solvents investigated. In addition, because sodium chloride (NaCl) drives Q11 assembly,³⁸ the significantly higher solubility of NaCl in methanol when compared to the other non-solvents investigated may dilute the concentration of ions in proximity of Q11 nanofibers, thereby inhibiting their physical crosslinking. However, these proposed mechanisms do not account for the irregular shape resulting from desolvation in isopropanol, which has the lowest dielectric constant and NaCl solubility. Instead, microgel shape irregularity may arise from the

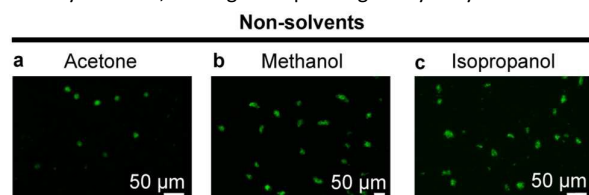


Figure 3. Influence of non-solvent on microgel fabrication. Fluorescent photomicrographs of ThT-stained microgels immediately after Q11 nanofiber desolvation in (a) acetone, (b) methanol, and (c) isopropanol.

higher viscosity of isopropanol when compared to the other non-solvents, which could reduce the shearing forces experienced by nanofibers under stirred conditions. Finally, the observed differences in the quality of fabricated microgels may also be related to differences in Q11 partitioning in each of these water/non-solvent pairs. Nonetheless, flexibility in the choice of ethanol or acetone as the non-solvent for Q11 may ultimately prove useful for specific applications, such as fabricating microgels loaded with therapeutics that are soluble or unstable in ethanol but not acetone. In addition, modifying desolvation parameters, such as PBS:non-solvent ratio or mixing speed, may lead to improved microgel fabrication via methanol or isopropanol. Owing to its effectiveness as a Q11 non-solvent and its use as an excipient in many existing drug formulations, ethanol was exclusively used as the non-solvent for the remainder of this report.

Finally, we assessed if microgels could be fabricated via desolvation with different synthetic β -sheet fibrilizing peptides (Figure 4). Similar to Q11, RADA16 and KFE8 self-assemble into β -sheet nanofibers under aqueous conditions, form physically crosslinked hydrogels above critical concentrations, and are zwitterionic at neutral pH.^{39, 40} RADA16 nanofibers appeared as amorphous fluorescent flocculates when stained with ThT in PBS and fluorescent microgels in ethanol immediately following desolvation (Figure 4a), similar to Q11 (Figure 1b-c). Some RADA16 microgels were retained following centrifugation and resuspension in PBS, while others appeared to dissociate (Figure 4a, right),

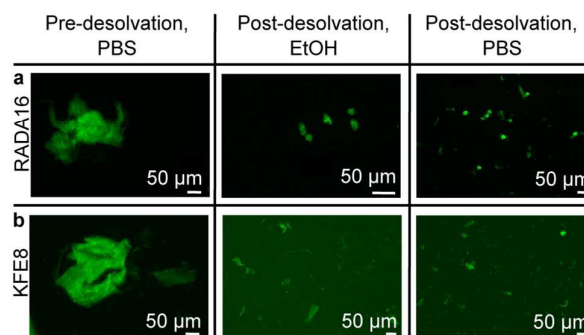


Figure 4. Fabrication of microgels via desolvation of RADA16 or KFE8 nanofibers. Fluorescent photomicrographs of ThT-stained (a) RADA16 or (b) KFE8 nanofibers prior to desolvation ("Pre-desolvation, PBS", left), microgels immediately after nanofiber desolvation ("Post-desolvation, EtOH", center), and microgels after centrifugation and resuspension in PBS ("Post-desolvation, PBS", right).

suggesting that physical crosslinking of RADA16 microgels may be less robust than that of Q11 microgels. KFE8 nanofibers also appeared as amorphous fluorescent flocculates when stained with ThT in PBS, yet desolvation of KFE8 with ethanol led to larger particulates with irregular morphologies (Figure 4b), similar to desolvation of Q11 with methanol (Figure 3b). Together, these data demonstrated that desolvation was not unique to Q11 and may provide a general method to fabricate microgels from various synthetic β -sheet fibrillizing peptides. Notably, however, the observation that desolvation was not uniform across all peptides suggests that the partitioning properties of nanofibers in water/non-solvent mixtures is dependent on the peptide primary sequence. Thus, on one hand, choosing the ideal non-solvent for a particular peptide will be more complicated than consideration of general solvent properties. However, on the other hand, opportunities may exist for achieving optimal desolvation with a particular non-solvent by modifying the primary sequence of the peptide, which could provide unique opportunities to encapsulate drugs that are unstable in particular solvents or have complex miscibility properties.

2.2 Q11 Microgel biocompatibility

Here we used *in vitro* dendritic cell activation as a preliminary assessment of Q11 microgel biocompatibility (Figure 5). Immature murine bone marrow-derived dendritic cells (DCs) treated with lipopolysaccharide significantly up-regulated expression of co-stimulatory markers (CD80 and CD86) (Figure 5a-b, supplemental figure 3) and cytokines (IL-12p70 and IL-27p28) (Figure 5c-d) that are associated with an inflammatory DC phenotype when compared to untreated cells. In contrast, DCs treated with Q11 microgels did not induce up-regulation of CD80, CD86, IL-12p70, or IL-27p28 expression (Figure 5a-d, Supplemental Figure 3). Taken together, these data demonstrated that Q11 microgels fabricated via desolvation did not induce DC activation to an inflammatory phenotype. This observation is consistent with reports demonstrating that Q11 nanofibers are minimally inflammatory *in vivo*,⁹ and suggests that Q11 microgels retain the immunogenicity profile of Q11 nanofibers. Thus, Q11 microgels are expected to be biocompatible, an essential criterion for effective protein drug delivery vehicles.

2.3 Protein encapsulation and release from Q11 microgels

To demonstrate the potential of Q11 microgels fabricated via desolvation as protein drug delivery vehicles, we first characterized the encapsulation and release of a model protein drug, super-folder green fluorescent protein (sfGFP), mixed with Q11 nanofibers prior to desolvation (Figure 6). sfGFP provides a useful model for these studies because GFP variants show low non-specific binding to Q11,⁴³ and perturbation of its folded state can be easily and reliably determined via fluorimetry. Following desolvation of aqueous buffered mixtures of Q11 nanofibers and sfGFP according to the approach outlined in Figure 1a, an sfGFP band was apparent in samples of microgels lysed with TFA and subjected to electrophoresis (Figure 6a), suggesting that sfGFP was co-desolvated with Q11. The recovered Q11 microgels fabricated in the presence of sfGFP were also fluorescent (Figure 6b), suggesting that admixtures of sfGFP and Q11 nanofibers co-desolvated into microgels with active protein cargo. Fluorescence was diffuse throughout the microgels (Figure 6b), suggesting that sfGFP was encapsulated within microgels rather than adsorbed onto them.

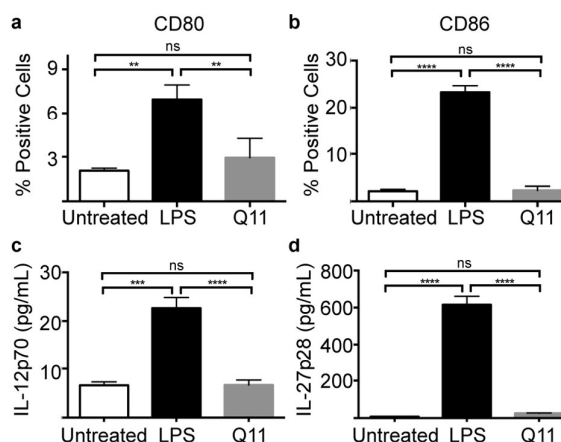


Figure 5. DC activation by Q11 microgels fabricated via desolvation. DC expression of (a) CD80 and (b) CD86. DC secretion of (c) IL-12p70 and (d) IL-27p28. “ns” denotes $p > 0.05$ between indicated groups, ** indicates $p < 0.01$, *** indicates $p < 0.001$, **** indicates $p < 0.0001$.

Fluorescent sfGFP rapidly diffused out from Q11 microgels into bulk aqueous media with typical burst release kinetics (supplemental figure 4), and the amount of sfGFP released could be tailored by varying the concentration of sfGFP mixed with Q11 nanofibers (Figure 6c). 85% of the total mass of active sfGFP mixed with Q11 nanofibers was released from the resultant microgels by 72 h, as determined fluorimetrically (Figure 6d). However, some sfGFP also remained within Q11 microgels, as determined by SDS-PAGE of TFA-lysed microgels at the endpoint of release (Figure 6e). Together, these data demonstrated that an active model protein drug, sfGFP, was efficiently encapsulated within Q11 microgels, and that a significant fraction of the encapsulated protein was subsequently released into bulk aqueous media and retained its activity. Future efforts will work towards modifying the fabrication methods to achieve complete release of encapsulated proteins, which may have been limited here by non-solvent partitioning effects or non-specific protein interactions with the microgel.

To further assess the potential of Q11 microgels as protein drug delivery vehicles, we characterized the encapsulation and release of wheat germ agglutinin (WGA), a plant lectin that induces agglutination and apoptosis of a human leukemic T cell line, Jurkat T cells.⁴⁸ Due to the rapid burst release of GFP from Q11 microgels, however, we sought to modify Q11 nanofibers in a manner that would enable tuning of WGA release kinetics. Toward this end, we characterized WGA release from microgels fabricated from multi-component nanofibers consisting of Q11 and a glycosylated Q11 variant developed previously by our group, n-acetylglucosamine-Q11 (GlcNAc-Q11), which binds reversibly to WGA with μM affinity.⁴¹ Microgels fabricated from an admixture of WGA and multi-component nanofibers of Q11 and GlcNAc-Q11 attenuated the burst release of WGA when compared to microgels fabricated from unmodified Q11 nanofibers (Figure 7a). Loading efficiency of WGA into mixed Q11/GlcNAc-Q11 microgels was comparable regardless of GlcNAc mole fraction (Supplemental Figure 5), and the magnitude of WGA burst release from GlcNAc-Q11 microgels decreased with increasing mole fraction of GlcNAc-Q11 integrated into nanofibers (Figure 7a). Together, these data suggested that loading efficiency was driven by the desolvation process, whereas release was modulated by protein-nanofiber binding affinity, which is dependent on the molar ratio of Q11 to GlcNAc-Q11.⁴¹ Notably,

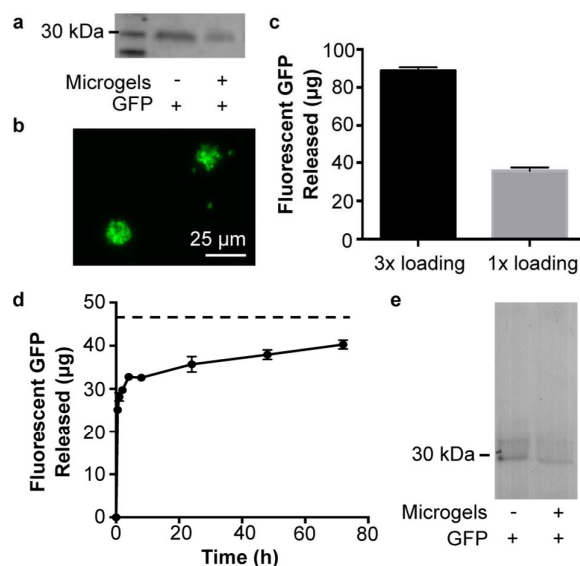


Figure 6. Super-folder green fluorescent protein (sfGFP) encapsulation and release from Q11 microgels fabricated via desolvation. a) SDS-PAGE gel of sfGFP stock (left) and sfGFP in Q11 microgels lysed with TFA (right). b) Fluorescent photomicrograph of microgels fabricated via desolvation of a Q11 nanofiber and sfGFP admixture. c) Extent of burst release of sfGFP from microgels fabricated from admixtures of Q11 and 141 μg sfGFP (“3x loading”) or 47 μg sfGFP (“1x loading”). d) Cumulative mass of fluorescent sfGFP released from Q11 microgels into bulk aqueous media (dashed line indicates total mass of sfGFP mixed with Q11 nanofibers prior to desolvation). e) SDS-PAGE gel of sfGFP stock (left) and Q11 microgels lysed with TFA at the end-point of sfGFP release (right).

the induction of Jurkat T cell apoptosis by WGA released from Q11 microgels was comparable to that of WGA that had not been subjected to desolvation (Figure 7b), suggesting that encapsulated protein bioactivity was retained during the microgel fabrication process. In addition, empty microgels did not induce Jurkat T cell apoptosis (Supplemental Figure 6), consistent with a previous report characterizing GlcNAc-Q11 nanofibers,⁴¹ suggesting that any residual non-solvent retained within Q11 microgels did not adversely affect their biocompatibility.

In longer studies, we observed that the mass of WGA released from microgels with 25% GlcNAc-Q11 reached a plateau between 8–24 h that persisted for at least 7 days, which corresponded to an extent of release of 51% (Figure 7c). In contrast, microgels with 0% GlcNAc-Q11 released increasing amounts of WGA over this same time frame, releasing 86% of the WGA mixed with Q11 nanofibers prior to desolvation over a 7-day period (Figure 7c). Notably, we observed similar release profiles from a different batch of WGA-loaded microgels having 0 or 25% GlcNAc-Q11 analyzed over a shorter time frame (Supplemental Figure 7), demonstrating that the observed release kinetics were relatively reproducible. Together, these data suggested that WGA-loaded microgels with 25% GlcNAc-Q11 may approach an equilibrium with the bulk aqueous phase in which the concentration of protein released is dependent on the WGA-GlcNAc dissociation constant, K_D . Consistent with this hypothesis, the mass of WGA released from microgels with 25% GlcNAc-Q11 increased or decreased in accordance with the volume of buffer that the microgels were maintained in during the course of the experiment, approaching

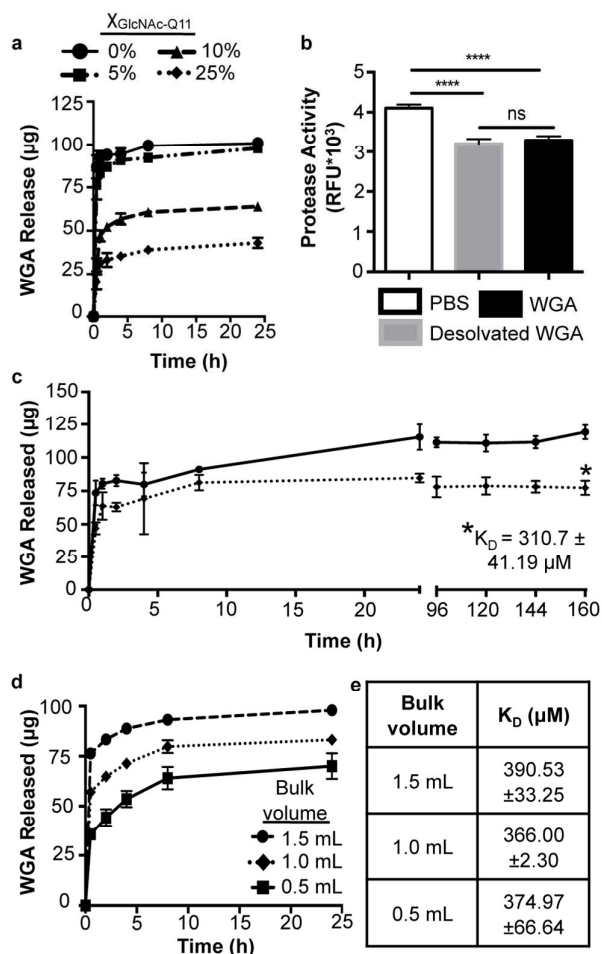


Figure 7. Tunable affinity-controlled release of wheat germ agglutinin (WGA) from Q11 microgels fabricated from nanofibers modified with a WGA-binding ligand, n-acetylglucosamine (GlcNAc-Q11). a) Burst release profiles of WGA from microgels fabricated from admixtures of WGA and Q11 nanofibers with 0% GlcNAc-Q11 (circles), 5% GlcNAc-Q11 (squares), 10% GlcNAc-Q11 (triangles), or 25% GlcNAc-Q11 (diamonds). b) Jurkat apoptosis induced by WGA released from Q11 microgels (gray), or stock WGA that had not been subjected to desolvation (black). “ns” denotes $p > 0.05$ between indicated groups, *** indicates $p < 0.001$, ANOVA with Tukey’s post-hoc. c) Long-term release profiles of WGA from microgels fabricated from an admixture of WGA and Q11 nanofibers with 0% GlcNAc-Q11 (circles) or 25% GlcNAc-Q11 (diamonds). d) Release of WGA from microgels fabricated from an admixture of WGA and Q11 nanofibers with 25% GlcNAc-Q11 into different volumes of bulk PBS. e) Dissociation constants, K_D , of microgels with 25% GlcNAc-Q11 for WGA.

plateaus at extents of release of 44%, 55%, and 69% for release into bulk volumes of 0.5, 1, or 1.5 mL, respectively (Figure 7d). Thus, as the slope of the WGA diffusion gradient out of the gels and into the bulk was decreased or increased, so was the extent of protein released, as expected for an affinity-controlled release system. Notably, the greater extent of WGA released into 1.5 mL PBS than

into 1 mL PBS (Figure 7c-d) suggested that the plateaus observed in the release profiles were not due to trapping of protein within the modified gels, either due to non-solvent partitioning or non-specific interactions with Q11 nanofibers, but rather due to the system approaching equilibrium. Further supporting this conclusion, the K_D calculated from concentration of WGA released, the concentration of GlcNAc-Q11, and the concentration of WGA retained within the microgels was ~ 350 - 400 μM in all release experiments (Figure 7e). It should be noted, however, that this observed K_D was ~ 15 -fold higher than that demonstrated for WGA binding to Q11/GlcNAc-Q11 nanofibers by our group previously,⁴¹ suggesting that some GlcNAc ligands may be inaccessible for WGA binding due to partitioning effects induced by the non-solvent or steric limitations imparted by the nanofibers. Future efforts may seek to improve ligand availability within the microgels by modifying the desolvation parameters or employing a different non-solvent. Nonetheless, these data demonstrated that modifying Q11 nanofibers with a protein-binding ligand can provide microgels with tunable affinity-controlled protein release profiles.

Taken together, these results demonstrated that proteins can be efficiently encapsulated within Q11 microgels by simply adding them to aqueous buffered solutions of Q11 nanofibers prior to desolvation. The bioactivity of two different model proteins, namely fluorescence of sfGFP and Jurkat T cell apoptosis via WGA, was maintained following desolvation, suggesting that exposure to non-solvent did not induce protein unfolding. In part, this may be due to peptide nanofibers having a lower activation energy for coacervation via desolvation than folded proteins, which leads to preferential aggregation and crosslinking of peptide nanofibers into microgels and in turn reduces protein susceptibility to unfolding or aggregation in the presence of a desolvating agent. The rapid burst release of sfGFP and WGA, which is also commonly observed with hydrogel networks that provide limited resistance to protein diffusion due to their highly hydrated and porous nature,³ suggested that Q11 microgels have some hydrogel-like properties that may also be advantageous for maintaining protein bioactivity. Notably, however, data in figure 7 also demonstrated that the rapid burst release from microgels of self-assembled peptide nanofibers can be attenuated by incorporating ligands that bind reversibly to proteins. This was consistent with previous reports demonstrating that ligands that bind to proteins either directly, or indirectly via heparin or biotin, can modulate the otherwise rapid burst release of therapeutic protein drugs from macroscopic hydrogels fabricated from self-assembled peptide nanofibers, thereby enhancing the efficacy of these biomaterials for tissue regeneration.^{19-23, 26} Here, the ability to easily and precisely tailor the concentration of ligand integrated into peptide nanofibers by simply mixing different Q11 variants in the pre-assembled state enabled tuning of protein release via a single protein-binding Q11 variant co-assembled with Q11 at different molar ratios (Figure 7a). This key feature of Q11 nanofibers can therefore eliminate the rather laborious process of identifying a panel of ligands having a range of protein-binding affinities that must be synthesized, purified, and installed into hydrogels at well-defined and reproducible concentrations to tailor protein release profiles, which is likely to hinder the development of hydrogels as protein delivery vehicles for widespread biomedical use. Yet, given that various different types of ligands, including peptides,¹⁰ proteins,⁴³ or carbohydrates,⁴¹ can be integrated into Q11 nanofibers at well-defined, tunable, and highly reproducible concentrations, it is expected that a broad range of protein-binding affinities and specificities can be achieved with this platform. Thus, the multitude of bio-inspired interactions that are often leveraged

to modulate protein drug release from biomaterials⁴⁴ are likely to be amenable to tailoring therapeutic cargo release from microgels of self-assembled peptide nanofibers in the future.

3. Experimental

3.1 Peptide Synthesis and Purification

RADA16 was purchased from Fisher Scientific (PuraMatrix®, 3-D Matrix Medical Technology, Waltham, MA, USA). The β -sheet fibrillizing peptides, Ac-QQKQFQFEQQ-Am (Q11), Ac-FKFEFKFE-NH₂ (KFE8), and NH₂-Asn(GlcNAc)-SGSG-Q11 (GlcNAc-Q11) were synthesized using established methods for standard Fmoc solid-phase peptide synthesis on a CS336X automated peptide synthesizer (CS Bio).^{38, 40, 41} All reagents for peptide synthesis were purchased from Novabiochem, unless stated otherwise. Peptides were cleaved and deprotected from synthesis resin by incubating in a cocktail of 9.5:0.25:0.25 trifluoroacetic acid (TFA) (Fisher):triisopropylsilane (TIS) (Sigma):water for 2.5 hours. Peptides were precipitated, washed with cold diethyl ether (Fisher), and dried *in vacuo*. Asn(Ac3NH- β -Glc)-SGSG-Q11 was deacetylated to give Asn(GlcNAc)-SGSG-Q11 by incubating the peptide in a sodium methoxide solution (0.5 M in methanol, pH 10) (Acros Organics) for 30 minutes. Peptide precipitate was sedimented by centrifugation, and sodium methoxide supernatant was decanted. Peptide pellet was then washed with methanol, and sedimented by centrifugation. Centrifugation and methanol washing steps were repeated twice. Finally, all peptides were dried *in vacuo*, dissolved in water, frozen, and lyophilized.

Peptides were purified to greater than 95% purity via reversed phase high performance liquid chromatography (RP-HPLC) using a Dionex™ Ultimate 3000™ System (Thermo Scientific) equipped with a C-18 column (Thermo Scientific) (supplemental figure 1). The mobile phase consisted of (A) water and (B) acetonitrile, both with 0.1% TFA. Elution was achieved with a linear gradient varying (B) from 25 to 35% over 10 min. Peptide was detected by absorbance at 215 nm. Peptide identities were confirmed with matrix-assisted laser desorption-ionization time-of-flight (MALDI-TOF) mass spectrometry (supplemental figure 1).

3.2 Nanofiber Preparation

To prepare nanofibers of Q11 and KFE8, lyophilized peptide powder was dissolved in deionized water at a concentration of 10 mM using alternating cycles of vortexing and sonication, and then allowed to incubate for 30 minutes at room temperature. Aqueous peptide solutions were then diluted to 0.1-1 mM in phosphate-buffered saline (PBS) (137 mM NaCl, 2.7 mM KCl, 10mM Na₂HPO₄ and 1.8mM KH₂PO₄) and incubated overnight at room temperature.

Mixed nanofibers of Q11/GlcNAc-Q11 were prepared using established peptide co-assembly methods.^{41, 42} Lyophilized peptide powders were mixed at varying ratios of Q11 to

GlcNAc-Q11 ($\chi_{\text{GlcNAc-Q11}} = 0.01, 0.05, 0.1, 0.25$, total Q11 = 10 mM). Peptide powders were co-dissolved in deionized water at a concentration of 10 mM using alternating cycles of vortexing and sonication, and then allowed to incubate for 30 minutes at room temperature. Aqueous peptide solutions were diluted in PBS and incubated overnight at room temperature.

RADA16 provided as an aqueous solution from the commercial supplier was diluted to 1mM in PBS and allowed to incubate overnight at room temperature prior to desolvation.

3.3 Microgel Preparation

Microgels were fabricated by diluting aqueous solutions of peptide nanofibers in a volumetric excess of non-solvent: ethanol (Fisher), methanol (Fisher), isopropanol (Fisher), or acetone (Fisher). Non-solvent was added dropwise to nanofiber solutions continuously stirred via a magnetic stir bar at 1150 rpm to a final ratio of 1:8 (v/v) non-solvent:PBS. Non-solvent:PBS mixtures were stirred for an additional 15 min at room temperature. Non-solvent:PBS mixtures were then centrifuged for 10 min at 3500 rpm in an Eppendorf MiniSpin, supernatant was removed, and pelleted microgels were resuspended in PBS by pipetting.

3.4 Electron Microscopy

For transmission electron microscopy, 0.1 mM Q11 nanofibers formed as described above were adsorbed on a formvar-carbon coated 400 mesh copper grid (FCF400-CU-UB, EMS) by floating the grids on 5 μL drops on parafilm for 1 min. Samples were negatively stained with 2% uranyl acetate in water, and analyzed using a Hitachi H-7000. Samples labeled "intact microgel" were adsorbed onto grids immediately after centrifugation and resuspension in PBS, while samples labeled "sheared microgel" were adsorbed onto grids after centrifugation, resuspension in PBS, and vortexing for 10 s.

For scanning electron microscopy, 0.5 mM Q11 nanofibers were desolvated into microgels using ethanol as the non-solvent as described above, except they were not centrifuged or resuspended in PBS. Instead, ethanolic solutions of microgels were spotted onto aluminum mounting stubs (EMS) painted with graphite, dried, sputter coated with a DeskV Sputter coater (Denton) under argon, and observed with a Hitachi S-4000 FE-SEM.

3.5 Thioflavin T staining

A 10 mM stock solution of Thioflavin T (ThT) (Sigma-Aldrich) in PBS was added to nanofibers at a ratio of 1:10 (v/v) to give a final ThT concentration of 1 mM. Mixtures of ThT and nanofibers or ThT and microgels were incubated for 20 min at room temperature to allow for ThT binding. ThT fluorescence intensity was analyzed using a BioTek Synergy plate reader equipped with 440/30 (excitation) and 485/20 (emission) filters.

3.6 Microgel Size Analysis

Aqueous solutions of Q11 (10 mM) were diluted to 0.1 mM, 0.25 mM, 0.5 mM, 0.75 mM and 1 mM in PBS and incubated overnight at room temperature. Q11 nanofibers were desolvated in ethanol as described above, stained with ThT as described above, and mounted onto glass microscope slides. ThT-stained microgels were then visualized with a Zeiss Axio Observer inverted epifluorescent microscope using GFP filters. Microgel diameter was measured using ImageJ then plotted and analyzed in Prism (Graphpad Software, La Jolla, CA USA). 100 microgels were analyzed per condition.

3.7 Circular Dichroism

Circular dichroism was performed on an Aviv 430 circular dichroism spectrometer (Aviv Biomedical, Lakewood, NJ). Q11 nanofibers and microgels were prepared as described above, except modified phosphate buffer (137 mM KF, 2.7 mM KCl, 10mM Na_2HPO_4 and 1.8mM KH_2PO_4) was used in place of PBS to eliminate background signal from chloride ions, similar to established methods.⁴³ 200 μM Q11 nanofibers, or 200 μM Q11 nanofibers desolvated into microgels, were analyzed 10 times with the average of these spectra reported as Mean Residue Ellipticity (MRE) vs wavelength. Analysis was completed in Prism (Graphpad Software, La Jolla, CA USA).

3.8 Zeta Potential

Zeta potential was measured with a BI-90 Plus zeta potential analyzer (Brookhaven Instruments, Holtsville, NY). The zeta potential measurements were obtained by diluting 1 mM solutions of Q11 nanofibers or microgels, prepared as described above, 30-fold in a 1 mM KNO_3 solution (pH 7.2). Each sample was analyzed 10 times, with the average and standard deviation reported.

3.9 Protein Loading and Release

Wheat germ agglutinin (WGA) was purchased from a commercial source (MP Biomedicals, LLC). Superfolder GFP (sfGFP) was recombinantly expressed in-house in *E. coli* hosts using established methods for metal-affinity purification.⁴⁴ 20 μM WGA or sfGFP were added to PBS solutions containing 1 mM Q11 nanofibers with $\chi_{\text{GlcNAc-Q11}} = 0, 0.01, 0.05, 0.1, \text{ or } 0.25$. Mixtures of proteins and nanofibers were co-desolvated via dilution in ethanol using methods described above.

sfGFP or WGA loading into microgels was analyzed with SDS-PAGE gel electrophoresis. Specifically, microgels in ethanolic desolvating solution were centrifuged at 3500 rpm for 10 min on an Eppendorf MiniSpin and supernatant was removed. Microgels were lysed via addition of 20 μL trifluoroacetic acid (TFA), followed by dilution with 200 μL "native buffer" (25 mM Tris + 192 mM glycine). TFA was then neutralized via addition of 2 N NaOH. 25 μL of lysis sample was then mixed with 25 μL 2x Laemmli sample buffer (Bio-Rad) and loaded into one well of a commercial pre-cast SDS-PAGE gel

(Bio-Rad AnyKD). To qualitatively assess protein-loading efficiency, an sfGFP stock subjected to similar lysis conditions was loaded into a neighboring well. Samples were electrophoretically separated at 100 V for 45 min. Gels were stained with Coomassie dye using conventional methods.

sfGFP loading into microgels was also assessed with fluorescence microscopy. Specifically, microgels in ethanolic desolvating solution were centrifuged at 3500 rpm for 10 min in an Eppendorf MiniSpin and supernatant was removed. Microgels were resuspended in PBS, mounted onto glass microscope slides, and visualized with a Zeiss Axio Observer inverted epifluorescent microscope using GFP filters.

To assess protein release, microgels in ethanolic desolvating solution were centrifuged at 3500 rpm for 10 min in an Eppendorf MiniSpin and supernatant was removed. Microgels were then resuspended in PBS at a final concentration of 0.2 mM Q11. At various time points, microgels were centrifuged for 10 min at 3500 rpm in an Eppendorf MiniSpin, and 50 μ L of supernatant was collected and analyzed for protein content. Following supernatant removal, 50 μ L of PBS was added back into the system. sfGFP release was determined fluorimetrically using a BioTek Synergy plate reader equipped with 485 nm (excitation) and 528 nm (emission) filters. WGA release was determined via tryptophan fluorescence (excitation: 280 nm/emission: 345 nm) using a SpectraMax M5 plate reader based on established methods.⁴¹ Protein fluorescence intensity was converted to protein concentration based on curves of fluorescence intensity of known standards. As described above for assessing microgel loading, residual GFP within microgels was measured using SDS-PAGE stained with Coomassie dye.

3.10 Dendritic Cell Isolation and Culture

All mouse procedures were performed in accordance with the approved guidelines set forth by the Institutional Animal Care and Use Committee at the University of Florida (Gainesville, FL, USA). Bone marrow derived progenitor cells were isolated from 8 to 12 week old C57BL/6J mice. Mice were euthanized via CO₂ asphyxiation followed by cervical dislocation. Tibias and femurs were harvested, and the shafts of the bones were flushed with cold PBS via a 27-gauge needle. The collected marrow suspension was centrifuged at 1250 rpm for 5 minutes. Next, the cells were resuspended in ACK lysis buffer (150mM NH₄Cl, 10 mM KHCO₃, 0.1 mM Na₂EDTA) to remove red blood cells. After lysis, cells were filtered through a 70 μ m Nydex cap (Becton Dickinson, NJ, USA) and recovered via centrifugation at 1250 rpm for 5 minutes. Finally, the cells were resuspended in complete DC media [RPMI 140 supplemented with 10% Fetal Bovine Serum (FBS) (Hyclone); 1% sodium pyruvate (HyClone); 1% non-essential amino acids (Lonza, Walkersville, MD, USA); 1% penicillin-streptomycin (Gibco); 1x L-Glutamine (200 mM) (HyClone); 10 ng/mL GM-CSF (PeproTech, Rocky Hill, NJ, USA); and 10 ng/mL IL-4 (PeproTech, Rocky Hill, NJ, USA)] and plated on 6-well ultra-low-cluster plates (Corning, Corning, NY). Cells were grown at

37°C in 5% CO₂ for 7-11 days. Media was removed and replaced with fresh complete DC media on days 3 and 5.

3.11 Dendritic Cell Maturation Studies

DC maturation was analyzed by assessing expression of surface markers via flow cytometry and release of cytokines with ELISA. After 7-11 days of culture, dendritic cells were treated for 24 h with 100 ng/mL lipopolysaccharide (LPS) (Invivogen) (positive control), 10 μ M Q11 microgels, or PBS ("untreated" negative control). At the incubation end-point, media supernatants were collected for ELISA analysis. Dendritic cells were removed from the culture plates with 5 mM Na₂EDTA in PBS (Hyclone). Next, the cells were washed with 1% FBS in PBS, and incubated with mouse CD16/CD32 for 30 minutes to block Fc γ receptors. Cells were then washed and stained with antibodies against CD80 (clone 16-10A1) (BD Pharmingen), CD86 (clone GL1) (BD Pharmingen) and CD11c (clone N418) (Biolegend) for 30 min at 4 °C. Data were acquired using flow cytometry (FACScalibur, Becton Dickinson, NJ, USA) and greater than 10,000 events were acquired for each sample. Data analysis was performed using FCS Express version 3 (De Novo Software, Los Angeles, CA, USA). Cell supernatant was analyzed for IL-12p70 and IL-27p28 using commercial murine ELISA assays (R&D systems, Minneapolis, MN, USA) as per manufacturer's instructions. ELISA results were analyzed using Prism (Graphpad Software, La Jolla, CA USA).

3.12 Jurkat T Cell Apoptosis Assay

Bioactivity of WGA released from Q11 microgels was assessed via induction of Jurkat T cell apoptosis. Briefly, Jurkat T cells (ATCC) (a generous gift from Dr. Mark Wallet) were plated in a 96-well plate at 10,000 cells/well in 40 μ L of "Complete Jurkat Media" (RPMI 140 supplemented with 10% Fetal Bovine Serum (FBS) (Hyclone), 1% penicillin-streptomycin (Gibco), 1x L-Glutamine 200mM (HyClone), 1% HEPES buffer (Hyclone). 1 mM Q11 nanofibers were co-desolvated with 20 μ M WGA as described above. After desolvation, WGA-loaded microgels were resuspended at a final concentration of 0.2 mM Q11 in PBS and were allowed to release WGA into the surrounding PBS for 24 hours at room temperature. In parallel, stock WGA was allowed to incubate at room temperature. After 24 hours, the microgels were sedimented, the supernatant was collected and the WGA concentration was measured using a SpectraMax M5 plate reader as described above. Released WGA and stock were added to the Jurkat T cells at a concentration of 6 μ g/mL. Next, 100 μ L of CellTiter-Fluor™ Reagent (Promega, Madison, WI) was added to each well. After 3 hours, Jurkat T cell protease activity, a relative measure of cell viability, was assessed by measuring CellTiter-Fluor fluorescence using a SpectraMax M5 plate reader at 385 nm (excitation) and 505 nm (emission). Protease activity was reported in RFU. Data was analyzed using Prism (Graphpad Software, La Jolla, CA USA).

3.13 Statistical Analysis

All experimental and control groups had at least $n=3$ for the sfGFP release, WGA release, GlcNAc-Q11 + WGA Release, Jurkat apoptosis, and dendritic cell activation studies. Data was analyzed for statistically significant differences using one-way ANOVA with Tukey's post-hoc ($p=0.05$) in GraphPad Prism software.

Conclusions

Microgels can be fabricated from nanofibers of synthetic peptides that self-assemble into β -sheets via desolvation, a simple 3-step batch process that utilizes conventional laboratory equipment. Nanofiber secondary structure was retained following desolvation, peptide feedstocks were integrated into microgels in high yield, and microgels were stable in aqueous buffers (Figure 1). Microgel size can be tuned by varying peptide concentration (Figure 2), various non-solvents can be used for microgel fabrication (Figure 3), and desolvation is amenable to different synthetic β -sheet fibrillizing peptides (Figure 4). Microgels do not induce DC activation to inflammatory phenotypes (Figure 5), or affect Jurkat T cell viability (Supplemental Figure 6), suggesting that they are biocompatible. Protein-loaded microgels can be fabricated via desolvation of aqueous admixtures of peptide nanofibers and proteins (Figure 6-7). Efficiency of protein encapsulation into microgels via desolvation was high, protein bioactivity was maintained, and protein release profiles could be modulated by modifying peptide nanofibers with protein-binding ligands. Owing to the potential for minimally-invasive delivery of protein-loaded microgels fabricated from self-assembled peptide nanofibers, we envision that these materials will be broadly useful as vehicles for protein drug delivery in various biomedical applications, including immunomodulation, cancer treatment, and viral infection prophylaxis.

Acknowledgements

This work was supported by the National Science Foundation (CAREER DMR-1455201) and start-up funds from the University of Florida. The authors would like to acknowledge the UF ICBR Electron Microscopy Core Facility for assistance with SEM sample preparation and data collection. The authors would also like to acknowledge Kevin Knox for assistance with peptide synthesis and purification. The authors would also like to acknowledge Andreina Chiu Lam and Dr. Carlos Rinaldi for assistance with zeta potential measurements. The authors would also like to acknowledge Dr. Mark Wallet for providing Jurkat T cells. The authors would also like to acknowledge Dr. Mavis Agbandje-McKenna and Dr. Robert McKenna for providing access to the CD spectrometer in the UF Center for Structural Biology.

References

- 1 R. A. Rader, *BIOPHARMA: Biopharmaceutical Products in the U.S. and European Markets*, 2013.
- 2 B. Leader, Q. J. Baca and D. E. Golan, *Nat Rev Drug Discov*, 2008, **7**, 21-39.
- 3 T. Vermonden, R. Censi and W. E. Hennink, *Chem Rev*, 2012, **112**, 2853-2888.
- 4 Y. Loo, S. Zhang and C. A. Hauser, *Biotechnol Adv*, 2012, **30**, 593-603.
- 5 H. Cui, M. J. Webber and S. I. Stupp, *Biopolymers*, 2010, **94**, 1-18.
- 6 M. J. Webber, E. A. Appel, E. W. Meijer and R. Langer, *Nature Materials*, 2016, doi:10.1038/nmat4474.
- 7 X. Du, J. Zhou, J. Shi and B. Xu, *Chem Rev*, 2015, **115**, 13165-13307.
- 8 G. A. Hudalla and J. H. Collier, in *Mimicking the Extracellular Matrix: The Intersection of Matrix Biology and Biomaterials*, eds. G. A. Hudalla and W. L. Murphy, Royal Society of Chemistry, London, 2015.
- 9 J. Chen, R. R. Pompano, F. W. Santiago, L. Maillat, R. Sciammas, T. Sun, H. Han, D. J. Topham, A. S. Chong and J. H. Collier, *Biomaterials*, 2013, **34**, 8776-8785.
- 10 J. P. Jung, A. K. Nagaraj, E. K. Fox, J. S. Rudra, J. M. Devgun and J. H. Collier, *Biomaterials*, 2009, **30**, 2400-2410.
- 11 L. A. Haines-Butterick, D. A. Salick, D. J. Pochan and J. P. Schneider, *Biomaterials*, 2008, **29**, 4164-4169.
- 12 P. C. Hsieh, M. E. Davis, J. Gannon, C. MacGillivray and R. T. Lee, *J Clin Invest*, 2006, **116**, 237-248.
- 13 M. E. Davis, J. P. Motion, D. A. Narmoneva, T. Takahashi, D. Hakuno, R. D. Kamm, S. Zhang and R. T. Lee, *Circulation*, 2005, **111**, 442-450.
- 14 T. C. Holmes, S. de Lacalle, X. Su, G. Liu, A. Rich and S. Zhang, *Proc Natl Acad Sci U S A*, 2000, **97**, 6728-6733.
- 15 M. C. Branco, D. J. Pochan, N. J. Wagner and J. P. Schneider, *Biomaterials*, 2009, **30**, 1339-1347.
- 16 S. Koutsopoulos, L. D. Unsworth, Y. Nagai and S. Zhang, *Proc Natl Acad Sci U S A*, 2009, **106**, 4623-4628.
- 17 F. Gelain, L. D. Unsworth and S. Zhang, *J Control Release*, 2010, **145**, 231-239.
- 18 M. C. Branco, D. J. Pochan, N. J. Wagner and J. P. Schneider, *Biomaterials*, 2010, **31**, 9527-9534.
- 19 J. C. Stendahl, L. J. Wang, L. W. Chow, D. B. Kaufman and S. I. Stupp, *Transplantation*, 2008, **86**, 478-481.
- 20 L. W. Chow, L. J. Wang, D. B. Kaufman and S. I. Stupp, *Biomaterials*, 2010, **31**, 6154-6161.
- 21 S. S. Lee, B. J. Huang, S. R. Kaltz, S. Sur, C. J. Newcomb, S. R. Stock, R. N. Shah and S. I. Stupp, *Biomaterials*, 2013, **34**, 452-459.
- 22 S. S. Lee, E. L. Hsu, M. Mendoza, J. Ghodasra, M. S. Nickoli, A. Ashtekar, M. Polavarapu, J. Babu, R. M. Riaz, J. D. Nicolas, D. Nelson, S. Z. Hashmi, S. R. Kaltz, J. S. Earhart, B. R. Merk, J. S. McKee, S. F. Bairstow, R. N. Shah, W. K. Hsu and S. I. Stupp, *Adv Healthc Mater*, 2015, **4**, 131-141.
- 23 M. E. Davis, P. C. Hsieh, T. Takahashi, Q. Song, S. Zhang, R. D. Kamm, A. J. Grodzinsky, P. Anversa and R. T. Lee, *Proc Natl Acad Sci U S A*, 2006, **103**, 8155-8160.
- 24 S. Lindsey, J. H. Piatt, P. Worthington, C. Sonmez, S. Satheye, J. P. Schneider, D. J. Pochan and S. A. Langhans, *Biomacromolecules*, 2015, **16**, 2672-2683.
- 25 E. L. Bakota, Y. Wang, F. R. Danesh and J. D. Hartgerink, *Biomacromolecules*, 2011, **12**, 1651-1657.
- 26 M. J. Webber, X. Han, S. N. Murthy, K. Rajangam, S. I. Stupp and J. W. Lomasney, *J Tissue Eng Regen Med*, 2010, **4**, 600-610.
- 27 V. A. Kumar, N. L. Taylor, S. Shi, N. C. Wickremasinghe, R. N. D'Souza and J. D. Hartgerink, *Biomaterials*, 2015, **52**, 71-78.

- 28 H. Byssell, R. Mansson, P. Hansson and M. Malmsten, *Adv Drug Deliv Rev*, 2011, **63**, 1172-1185.
- 29 Y. F. Tian, J. M. Devgun and J. H. Collier, *Soft Matter*, 2011, **7**, 6005-6011.
- 30 U. Shimanovich, I. Efimov, T. O. Mason, P. Flagmeier, A. K. Buell, A. Gedanken, S. Linse, K. S. Akerfeldt, C. M. Dobson, D. A. Weitz and T. P. Knowles, *ACS Nano*, 2015, **9**, 43-51.
- 31 S. Bai, S. Debnath, K. Gibson, B. Schlicht, L. Bayne, M. Zagnoni and R. V. Ulijn, *Small*, 2014, **10**, 285-293.
- 32 S. Bai, C. Pappas, S. Debnath, P. W. Frederix, J. Leckie, S. Fleming and R. V. Ulijn, *ACS Nano*, 2014, **8**, 7005-7013.
- 33 Y. Tsuda, Y. Morimoto and S. Takeuchi, *Langmuir*, 2010, **26**, 2645-2649.
- 34 J. J. Marty, R. C. Oppenheim and P. Speiser, *Pharm Acta Helv*, 1978, **53**, 17-23.
- 35 A. O. Elzoghby, W. M. Samy and N. A. Elgindy, *J Control Release*, 2012, **161**, 38-49.
- 36 J. Kreuter, *Colloid Drug Delivery Systems*, Marcel Dekker, New York, NY, 1994.
- 37 C. Weber, C. Coester, J. Kreuter and K. Langer, *Int J Pharm*, 2000, **194**, 91-102.
- 38 J. H. Collier and P. B. Messersmith, *Bioconjug Chem*, 2003, **14**, 748-755.
- 39 S. Zhang, T. C. Holmes, C. M. DiPersio, R. O. Hynes, X. Su and A. Rich, *Biomaterials*, 1995, **16**, 1385-1393.
- 40 D. M. Marini, W. Hwang, D. A. Lauffenburger, S. Zhang and R. D. Kamm, *Nano Letters*, 2002, **2**, 295-299.
- 41 A. Restuccia, Y. F. Tian, J. H. Collier and G. A. Hudalla, *Cell Mol Bioeng*, 2015, **8**, 471-487.
- 42 J. Z. Gasiorowski and J. H. Collier, *Biomacromolecules*, 2011, **12**, 3549-3558.
- 43 G. A. Hudalla, T. Sun, J. Z. Gasiorowski, H. Han, Y. F. Tian, A. S. Chong and J. H. Collier, *Nat Mater*, 2014, **13**, 829-836.
- 44 G. A. Hudalla and W. L. Murphy, *Adv Funct Mater*, 2011, **21**, 1754-1768.
- 45 P. S. Vassar and C. F. Culling, *Arch Pathol*, 1959, **68**, 487-498.
- 46 S. Seiffert, *Chemphyschem*, 2013, **14**, 295-304.
- 47 R. M. Kramer, V. R. Shende, N. Motl, C. N. Pace and J. M. Scholtz, *Biophys J*, 2012, **102**, 1907-1915.
- 48 B. Gastman, K. Wang, J. Han, Z. Y. Zhu, X. Huang, G. Q. Wang, H. Rabinowich and E. Gorelik, *Biochem Biophys Res Commun*, 2004, **316**, 263-271.